Superhydrophobic Surface of AZ31 Alloy Fabricated by Chemical Treatment in the NiSO$_4$ Solution

M. Yeganeh, M. Omidi, and M. Eskandari

In the present study, the formation of superhydrophobic (SHP) structure on the surface of Mg alloy was investigated by immersion in the CuCl$_2$ and NiSO$_4$ solutions following by soaking in the stearic acid (SA) solution. The results revealed the presence of some stearic acid bonds on the surface of Mg alloy. The contact angle of the surface after the process measured about 151.5°, which could be due to the presence of flake-like morphology and the adsorption of hydrophobic substances of SA. X-ray diffraction pattern showed the presence of NiO as the resistant phase against the diffusion of species. Besides, the values of noise and corrosion resistance regarding SHP Mg were at least three orders of magnitude higher than that of bare Mg alloy due to the formation of SHP structure.

Keywords	corrosion, Mg alloys, superhydrophobic surfaces

1. Introduction

Magnesium alloys have shown special remarkable properties including high specific strength, low density, high thermal conductivity, excellent machinability, high damping capacity, good weldability under the controlled ambient, excellent castability, and recyclability. These alloys can be applied in the automotive, aerospace, electronics, medical, and other industries (Ref 1-3). However, the inherent poor electrochemical corrosion resistance of Mg alloys due to their low standard electrode potential is a major drawback for their applications (Ref 4, 5). Besides, magnesium possesses high chemical activity and the formed oxide film on the surface of its alloys is porous and non-protective under the natural state (Ref 6). Another problem is that the chemical activity of industrial magnesium alloys is mainly inhomogeneous. For instance, AZ91D magnesium alloy which has been extensively used in the automobile industries is made of α phase (Mg) and β phase (Mg$_{17}$Al$_{12}$) (Ref 7).Various surface treatment techniques have been used to reduce the chemical and electrochemical activity of magnesium including physical vapor deposition (Ref 8, 9), electroless plating (Ref 10-12), plasma electrolytic oxidation (PEO) (Ref 13-15), chemical conversion treatments (Ref 16-18), hydroxyapatite coatings (Ref 19-21), and the other coatings (Ref 22-24).

Surface modification of Mg alloys due to their high activity and inhomogeneity is difficult (Ref 7). Moreover, the formation of the corrosion products is quite complicated and not well understood. For example, when AZ91 Mg alloy is immersed in

aqueous solutions, the film on the surface of the α phase consists of three layers including the outer layer of Mg(OH)$_2$, the middle layer of MgO, and the inner layer of Al$_2$O$_3$. The formed surface film on the β phase is different from that on α phase which leads to the inhomogeneity of surface chemistry (Ref 9-11). Consequently, it is challenging to control the formation of corrosion products under the laboratory conditions (Ref 25, 26).

In recent years, fabrication of superhydrophobic surfaces has become an area of active fundamental research. In general, similar techniques used for micro- and nanostructure manufacturing, such as lithography, etching, chemical and electrochemical deposition, casting, plasma treatment, and replication have been used for producing superhydrophobic surfaces (Ref 27). There are two main requirements to fabricate a superhydrophobic surface: (1) the surface should be rough and (2) it should have a low surface energy. These two requirements lead to two methods of producing superhydrophobic surfaces. The first method is to make a rough surface from an initially hydrophobic material, and the second method is to modify an initially rough surface by changing the surface chemistry or applying a hydrophobic material (Ref 27-30). Few researchers have investigated on the SHPS of Mg. The investigated processes categorize on the basis of chemical, electrochemical or physical surface treatment including hydrothermal technique (Ref 31), chemical and electrochemical deposition (Ref 32-36), conversion coating (Ref 37, 38), polymer coating (Ref 39), and etching processes (Ref 40, 41).

The main aim of present study is to creation of a superhydrophobic surface of Mg alloy to protect its surface against corrosion in the aggressive media. Hence, AZ31 alloy was treated in the chemical solution of CuCl$_2$, NiSO$_4$, and stearic acid to form a corrosion-resistant superhydrophobic surface. On the other words, this work is a combination of chemical etching and chemical deposition of the protective compound. In current study, electrochemical behavior of SHP Mg including electrochemical impedance spectroscopy, potentiodynamic polarization, and electrochemical noise spectroscopy was studied. This surface of SHP Mg alloy showed excellent corrosion resistance with superhydrophobicity during 168 h.

M. Yeganeh and M. Eskandari, Department of Materials Science and Engineering, Faculty of Engineering, Shahid Chamran University of Ahvaz, Ahvaz, Iran; and M. Omidi, Advanced Materials Research Center, Department of Materials Engineering, Najafabad Branch, Islamic Azad University, Najafabad, Iran. Contact e-mails: m.yeganeh@scu.ac.ir and yeganeh.mahdi@gmail.com.

2. Experimental

2.1 Materials

AZ31 Mg alloy samples (3% aluminum and 1% zinc) with the dimension of 30 mm × 25 mm × 2 mm were used. Citric acid (99.5%—Samchun), copper chloride (99.8%—Merck), nickel (II) sulfate hexahydrate (extra pure—Samchun), stearic acid (99.7%—Merck), and ethanol (99%) were used without any further purification.

2.2 Sample Preparation

Magnesium plates were first abraded with SiC papers up to #2000 and then the plates were ultrasonicated in the methanol for 1 min and subsequently dried by immersion in the 100 ml of 2 wt.% to obtain a high surface activity. At the next stage, the samples were immersed in the 3.4 wt.% copper chloride in the aqueous solution at 90 °C for 5 min followed by immersion in the nickel (II) sulfate hexahydrate solution (0.8 g/100 ml H_2O) at 80 °C for 10 min. The obtained samples were immersed in the ethanolic solution of stearic acid ($CH_3(CH_2)_{16}COOH$) for 4 h at the room temperature. Finally, the samples were dried at 120 °C for 15 min.

2.3 Sample Characterization

The morphology of treated sample (SHP Mg) was studied with a high-resolution scanning electron microscope (CamScan Mira). Contact angles were measured by optical contact angle measuring device (Data physics OCA15 plus). X-ray diffraction (XRD) pattern of the superhydrophobic surface of Mg alloy was obtained by a Philips PW 1730 diffractometer using Cu Kα radiation (40 kV, 40 mA) in the range of 20°-90°. Fourier transform infrared (FTIR) spectroscopic analysis regarding the coatings was performed by Nicolet IR 100 using KBr disk. The scanning ranges were from 4000 to 500 cm^{-1}. The corrosion resistance of the SHP Mg and Mg alloy was tested using an AUTOLAB PGSTAT 30 potentiostat equipped with a three-electrode system with an Ag/AgCl reference electrode consisting of a saturated KCl solution, platinum as the counter electrode, and the sample (SHP Mg and Mg alloy) as the working electrode. Electrochemical impedance spectroscopy (EIS) was conducted in the frequency ranges from 100 mHz to 100 kHz with a perturbation amplitude sinusoidal signal of 10 mV. Corrosion properties of SHP Mg and Mg alloy 3.5 wt.% NaCl and deionized water solutions were investigated by electrochemical impedance tests at various times [1 h, 12 h, 1 day, and 1 week (168 h)]. Potentiodynamic polarization tests were performed in the potential ranges from − 300 to 400 mV versus Ag/AgCl. The scanning rate was set at 2 mV s^{-1}. Corrosion current density (i_{corr}) and corrosion potential (E_{corr}) were determined by NOVA software. The corrosion resistance of the working electrode (1 cm^2) was investigated in 3.5 wt.% NaCl and deionized water solutions. Three replications were tested to ensure repeatability of data. ZView 3.5c software was used to analyze EIS data.

Electrochemical noise (EN) analysis was conducted in the system containing two identical working electrodes of SHP Mg or Mg and a saturated Ag/AgCl as the reference electrode. These three electrodes were dipped in 3.5 wt.% NaCl solution. The potential and current noise data collected in the time domain were transformed to the frequency domain using the fast Fourier transform (FFT). The electrochemical noise data were recorded for 1024 s at immersion times of 1 h. All electrochemical corrosion measurements were repeated three times to verify the reproducibility of the results.

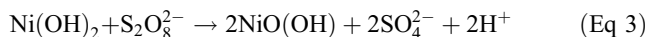## 3. Results and Discussion

Figure 1(a)-(d) shows FESEM morphology of Mg (a and b) and SHP Mg (c and d) surface with the different magnifications. In the case of Mg with lower magnification (Fig. 1a), the bright and dark phases stand for α-Mg and β-$Mg_{17}Al_{12}$ phases, respectively (Ref 7). Moreover, the measured contact angle corresponding to Mg alloy was 48°. In the case of SHP Mg, the flake-like morphology was observed after the immersion and modification of Mg surface, which could act as a barrier to the water droplets. As can be observed, the surface morphology after chemical treatment changed completely and composed of the porous and uniform flakes which were evenly distributed on the surface with a preferred direction. These flakes possessed the thickness in the range of 20-50 nm. These flakes could trap the air which led to the prevention of liquid penetration into the coated surface (Ref 42). The measured contact angle was about 151.5°, which depicted superhydrophobicity. The large contact angle between the water and air could prevent the penetration of water or aggressive species toward the surface according to Cassie–Baxter equation (Ref 43). It has been reported (Ref 44) that a robust micro/nanostructure is a key factor for a SHP surface. The hierarchical micro/nanoscaled structure supplied more space to capture the air to achieve superhydrophobicity.

Figure 2(a) and (b) demonstrates x-ray diffraction pattern and energy-dispersive spectroscopy (EDS) related to the SHP Mg. XRD pattern (Fig. 2a) displays the presence of Mg (JCPDS 35-0821), NiO (JCPDS 47-1049), and MgO (JCPDS 01-1235) on the surface of SHP Mg. The XRD patterns showed broad peaks about 37.8° which could be attributed to the (111) plane of NiO phase. That strong (111) plane might be the reason for the preferred direction of flake morphology of SHP Mg. Figure 2(b) illustrates EDS spectra corresponding to the SHP Mg surface. As it can be observed, the coating was constituted of Ni, Mg, S, and O. The presence of Mg could be attributed to the low thickness of chemical deposit and surface roughness. Sulfur and oxygen could arise from the solution during NiO deposition. Although, it shows copper acted as the etchant material and did not deposit on the surface.

Figure 3 shows the process of nickel deposition on the surface of Mg alloy. In the primary stage, the chemical activity of β ($Mg_{17}Al_{12}$) phase was lower than α (pure Mg) phase (Ref 45). Therefore, α phase dissolved earlier and supplied the Mg^{2+} cation and electrons. Then, the Ni^{2+} cations could react with the electrons and hydroxyl ions to form $Ni(OH)_2$ as follows:

$$2Ni^{2+} + 2e^- + 2OH^- \rightarrow 2Ni(OH)_2 \qquad \text{(Eq 1)}$$
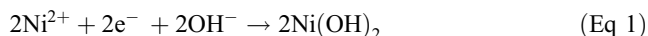
However, the formation of NiO might be influenced by the presence of sulfate in the solution as stated in some papers. These particles can react with persulfate ($S_2O_8^{2-}$) from $NiSO_4$ solution (Ref 46):

$$2SO_4^{2-} \rightarrow S_2O_8^{2-} + 2e^- \qquad \text{(Eq 2)}$$

$$Ni(OH)_2 + S_2O_8^{2-} \rightarrow 2NiO(OH) + 2SO_4^{2-} + 2H^+ \qquad \text{(Eq 3)}$$

This reaction could act as the rate-determining step in the growth of NiO film (Ref 46). Therefore, it can be mentioned
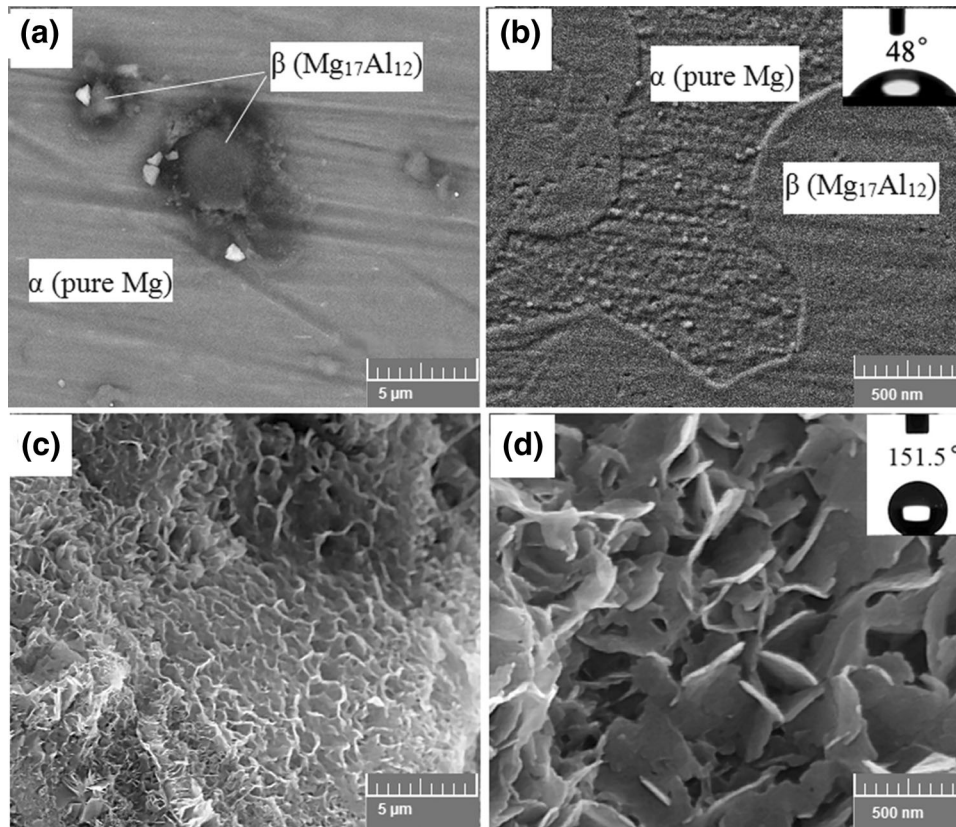
Fig. 1 Surface morphology of (a) Mg with low magnification, (b) Mg with high magnification, (c) SHP Mg with low magnification, (d) SHP Mg with high magnification with contact angle inside
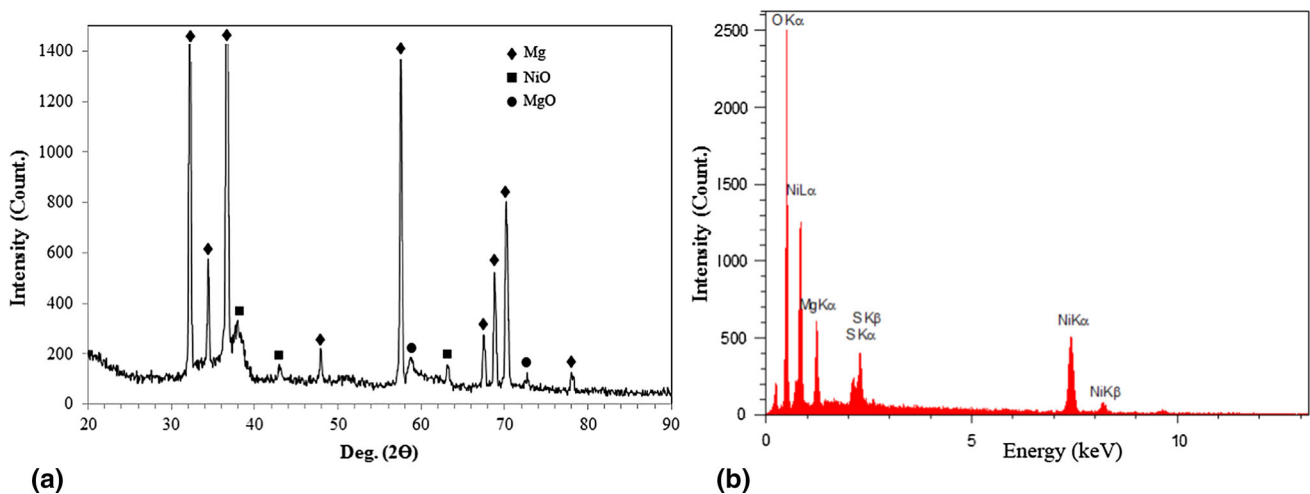

Fig. 2 (a) XRD pattern, and (b) EDS spectra regarding SHP Mg alloy

that the formation of NiO might be due to dehydration of $Ni(OH)_2$ or reaction with sulfate substances in the solution. The formed phase could deposit on α phase. Consequently, α phase was covered with NiO deposits and dissolution of Mg stopped. In the next stage, the β phase started to dissolve and the production of Mg^{2+} and Al^{3+} cations and electrons proceeded. Finally, α phase and β phase were deposited with NiO and the reaction reached the equilibrium. It could be known that the difference of chemical activity between α phase and β phase was the main

reason which led to the variation in the amounts of NiO deposition on the two phases and the appearance of the rough surface. In the etching process, the surface was corroded unevenly by chloride ions and the surface possesses higher roughness. In the next stage, Ni ions from $NiSO_4$ solution tended to deposit on the surface and finally a flake-like morphology was created on the uneven surface of Mg alloy.

Figure 4 depicts FTIR spectra of the stearic acid and SHP Mg. The asymmetric and symmetric stretching vibrations of C–

H peaks were located at about 2850 and 2920 cm^{-1}, which could be attributed to the presence of the aliphatic groups on the superhydrophobic surface arising from stearic acid. The observed band about 1105 and 1700 cm^{-1} could be related to the C=O and –COO groups, respectively. C–O and C–C bonds were detected about 1120 and 1635 cm^{-1}, respectively. Also, the band appears about 837 cm^{-1} indicating C–OR contributing to the superhydrophobic surface. Besides, the peaks at 2910 and 2860 cm^{-1} corresponded to the asymmetric and symmetric stretching vibrations of –CH$_2$ or –CH$_3$ groups (Ref 47-49). These adsorbing bonds corresponding to the SHP Mg could be attributed to the functional groups of SA indicating the presence of SA on the SHP surface. In fact, these observations suggested the formation of carboxylate (CH$_3$(CH$_2$)$_{16}$COO$^-$) on the Mg substrate.

Figure 5(a) and (b) shows Nyquist spectra corresponding to Mg alloy and SHP Mg alloy after different immersion times (1, 12, 24, and 168 h) in the 3.5 wt.% NaCl. In the case of Mg alloy, the semicircle plot which was related to the capacitive loop in the high–medium-frequency region was associated with the charge transfer resistance and the electric double-layer capacitance. Corrosion resistance (R_{ct}) was measured as the content of Z' when $-Z'' = 0$, which was usually calculated at the intermediate frequencies (Ref 24). In the case of SHP Mg, the inductive loop was disappeared which indicated the significant reduction in electrolyte penetration to the interface. The inductive loop can be explained by the different mechanisms including pitting, hydroxide formation, and adsorption (Ref 24). By surface modification of Mg alloy during the mentioned processes, the active surface of this alloy was kept away from chemical species and adsorbing ions. SHP Mg alloy showed two distinct time constants, in which the first was related to the coating resistance at the high-frequency domain

arising from chemical deposited film in the NiSO$_4$ containing solution. The second one was attributed to the charge transfer resistance at the low range frequency domain linked to the Mg charge transfer (Ref 24). Second semicircle occurred in the low-frequency domain of the Nyquist plots reflected the electrochemical reaction under the coating. As immersion time was prolonged, the radius of semicircle decreased, indicating the reduction in the charge transfer resistance (R_{ct}) and permeation of aggressive ions to the interface (Ref 24, 45). By passing the time, diameter of the loop related to charge transfer resistance decreases, implying the diffusion of aggressive species through the NiO layer.

Figure 6(a) and (b) shows equivalent circuits corresponding to Mg alloy and SHP Mg alloy, respectively. These models include the solution resistance R_s, a series combination of resistance, R, and inductance, L, in parallel with charge transfer resistance R_{ct}, and the constant phase element (CPE). CPE was used instead of a pure capacitance (C) accounting for non-ideal capacitive response of the interface. The impedance of a CPE is equal to $A^{-1}(i\omega)^{-n}$, where A is the constant corresponding to the interfacial capacitance, i is the imaginary number, ω is the angular frequency, and n is an exponential factor in the range between -1 and 1. Depending on the value of n, CPE can illustrate resistance ($n = 0$, $A = R$), capacitance ($n = 1$, $A = C$), inductance ($n = -1$, $A = L$), and Warburg impedance ($n = 0.5$, $A = W$) in the different situations. Pure capacitance behavior is indicated by $n = 1$, while in practice n often ranges from zero to 1. Heterogeneity of the water diffusion phenomenon could impose deviation from the pure capacitor (Ref 24, 50, 51, and 52). Besides, n is associated with the degree of roughness and the geometry of the coatings (Ref 50). Table 1 shows the obtained parameters from simulation by ZView software. The proposed equivalent circuits fitted very well emphasized by the low value of χ^2, which is one of the most important parameters in the curve fitting process (Ref 45, 50). The reported values regarding χ^2 were less than 0.01 for all specimens. R_{ct} for Mg alloy after immersion at 1 h, 12 h, 24 h, and 1 week was obtained as 290, 110, 75, and 52 Ω cm^2, respectively. This parameter for SHP Mg alloy at the same times reported as 1500, 1100, 950, and 640 kΩ cm^2, which could be explained by the effect of superhydrophobicity behavior on the surface of Mg alloy. According to the reported data, corrosion resistance regarding SHP Mg was at least four orders of magnitude higher than that of for bare Mg alloy at each time of immersion. The significant corrosion resistance of SHP Mg alloy can be due to the presence of superhydrophobic surface with the flake-like morphology and the adsorption of low energy substances of stearic acid (Ref 28).

According to Table 1, R_c (coating resistance) value reduced from 3010 to 700 kΩ cm^2 for SHP Mg alloy, while Mg alloy showed no obvious time constant related to the coating resistance. In other words, R_c regarding SHP Mg alloy has been appeared due to the barrier properties of NiO compound. Besides, the observed reductions in the R_c values show the degradation of coatings by chloride or hydroxyl ion penetration. By passing the time, coatings showed the higher affinity to the aggressive ions and displayed higher conduction. In other words, the observed decrease in the R_c or increase in CPE$_c$ values was attributed to the accumulation of conducting species in the porosities of the coatings (Ref 24). Similarly, CPE is related to the corrosion reaction area, i.e., low CPE implies that relatively low area of the exposed surface is corroded. The fitted values of CPE showed a continuous decrease in the
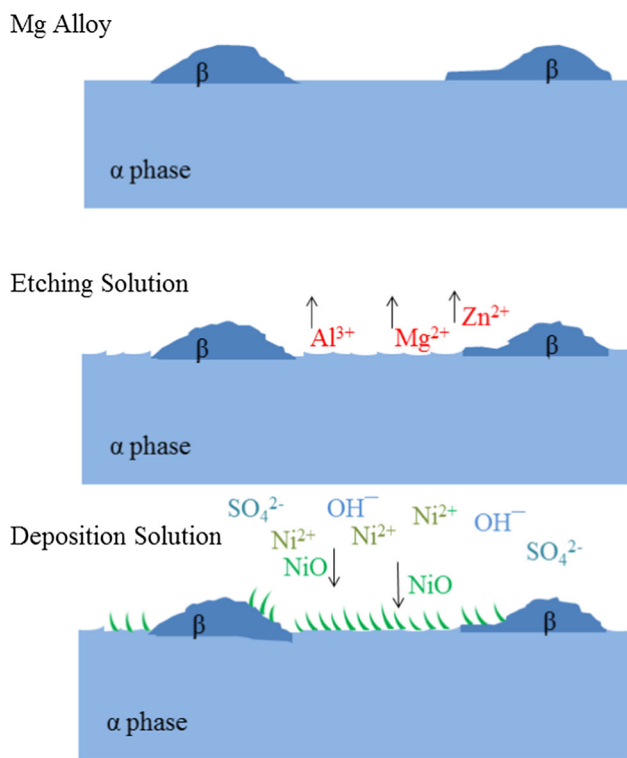

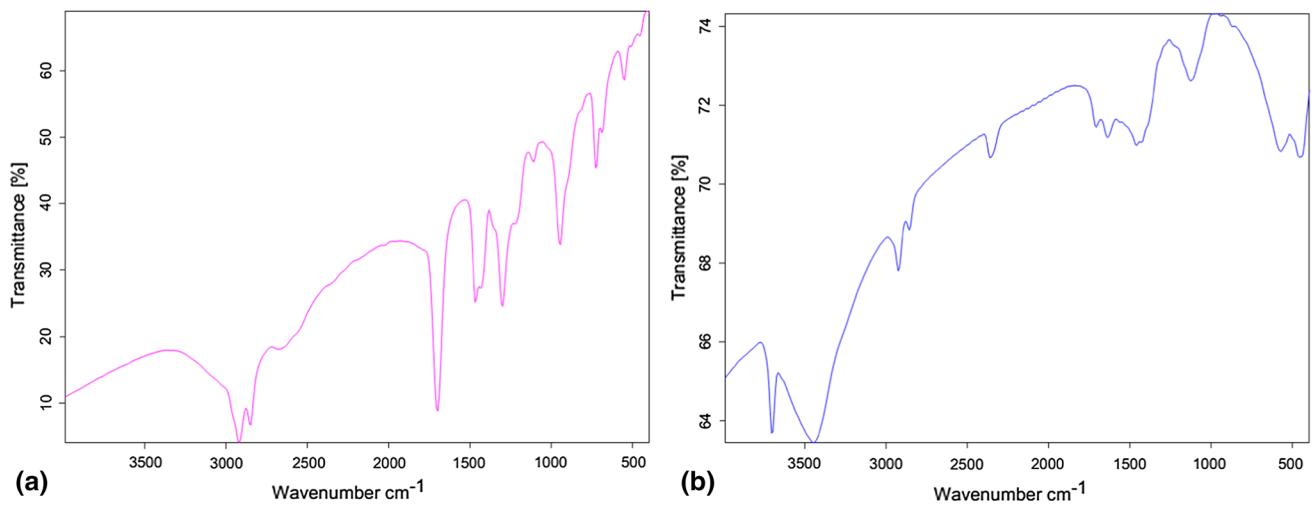**Fig. 3** Schematic process to make superhydrophobic surface

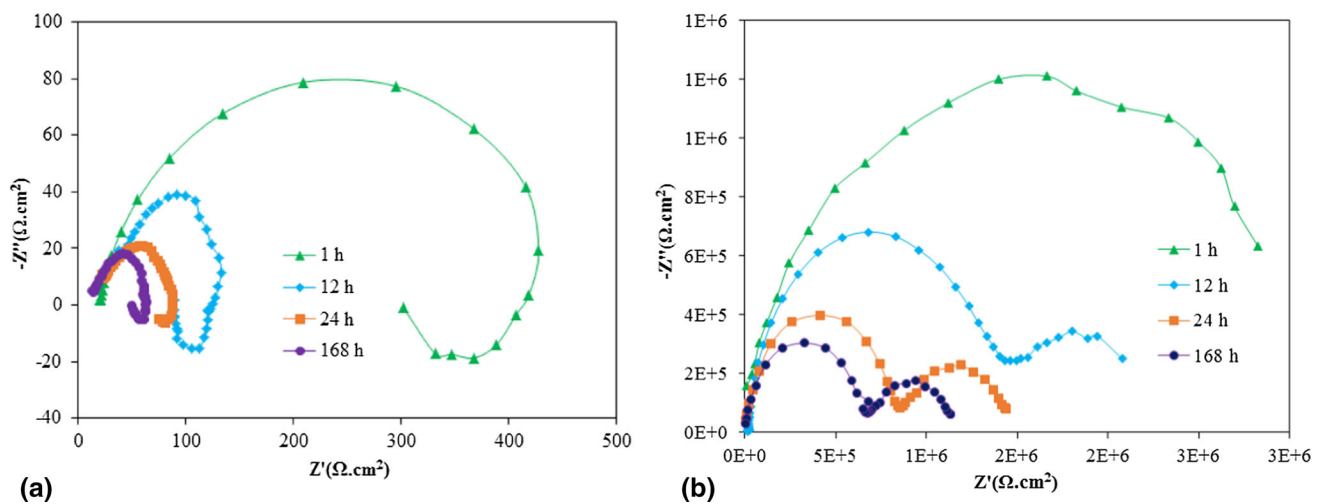**Fig.4** FTIR spectra of the (a) stearic acid (SA) and (b) superhydrophobic Mg (SHP Mg)

Fig. 5 Nyquist plots regarding (a) Mg alloy and (b) SHP Mg alloy after different times of immersion in the 3.5 wt.% NaCl
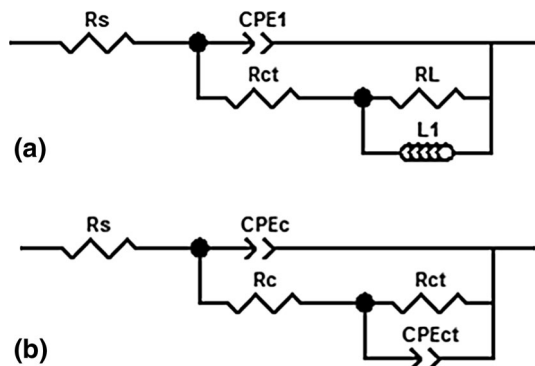

Fig. 6 Equivalent circuits for (a) Mg alloy and (b) SHP Mg alloy in 3.5 wt.% NaCl solutions

double-layer coating capacitance. The values of n (CPE-P) for all the coatings were closer to unity, indicating a capacitance behavior. However, the deviation observed in the n values was normally arising from the heterogeneity in the coating or water diffusion, which led to the non-uniform current distribution

(Ref 53, 54). Although, bare Mg alloy showed inductor element (L) in the low-frequency region. This parameter varied from 145.5 to 62.5 H during the immersion, which could be a sign of a decrease in the induction behavior due to the formation of corrosion products and reduction in active surface exposing the electrolyte.

Table 2 represents two important parameters corresponding to the corrosion properties. $|Z|_{100 \text{ mHz}}$ and $\theta_{10 \text{ kHz}}$ are suitable parameters to determine the electrochemical properties of the coated surface (Ref 24). If these parameters possess the higher values, corrosion resistance regarding the samples would be greater. Impedance magnitude at 100 mHz ($|Z|_{100 \text{ mHz}}$) and phase angle at 10 kHz ($\theta_{10 \text{ kHz}}$) emphasize the qualitative behavior regarding the corrosion phenomena. If charge transfer resistance and/or double-layer capacitance values are significant, the electrochemical behavior of metal–electrolyte interface will become capacitive. In this case, the current would principally cross through the capacitor and, therefore, the value of phase angle reaches about 90°. In addition, if resistance and/or capacitance values are negligible, the electrochemical response of the metal–electrolyte interface will turn resistive. Consequently, the current would frequently pass through the

Table 1 Impedance data regarding Mg alloy and SHP Mg alloy at different times of immersion in the NaCl solution

	Time, h	R_c, kΩ cm²	CPE$_c$-T, nF	CPE$_c$-P, nF	R_{ct}, kΩ cm²	CPE$_{ct}$, nF	L (H)	$χ^2$
Mg alloy	1	...	...	0.78	0.330		145.5	0.0001
	12	...	...	0.67	0.110		75.2	0.01
	24	...	...	0.71	0.075		60.8	0.002
	168	...	...	0.65	0.052		62.5	0.005
SHP Mg alloy	1	3010	0.17	0.81	1500		...	0.004
	12	2101	0.19	0.71	1100		...	0.003
	24	900	0.25	0.75	950		...	0.001
	168	700	0.46	0.67	640		...	0.005

Table 2 Impedance parameters for SHP Mg and Mg alloy at different immersion times in the NaCl solution

Sample	Time, h	$|Z|_{100\ mHz}$, MΩ cm²	$θ_{10\ kHz}$, °	Sample	Time, h	$|Z|_{100\ mHz}$, Ω cm²	$θ_{10\ kHz}$, °
SHP Mg alloy	1	2.5	81	Mg alloy	1	290	7
	12	2.1	75		12	110	6.5
	24	1.6	73		24	80	6.8
	168	1.1	70		168	65	2

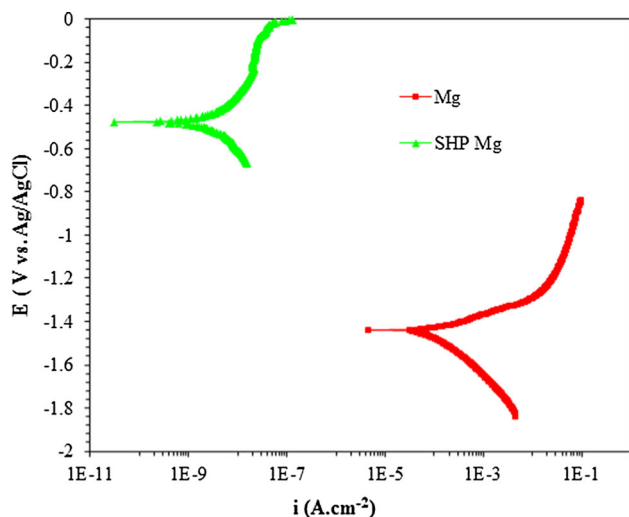**Fig. 7** Potentiodynamic polarization plots regarding SHP Mg alloy and Mg alloy after immersion of 1 h in the 3.5 wt.% NaCl

Fig. 8 Power spectral density (PSD) of current for SHP Mg alloy and Mg alloy measured after 1 h of immersion in 3.5 wt.% NaCl solution

resistor, and therefore, the value of phase angle would be close to 0° (Ref 24, 55). According to Table 2, the maximum obtained value related to the phase angle at 10 kHz ($θ_{10\ kHz}$) was about 81°. It was reported that the value of $θ$ for intact coatings is close to 90° (Ref 24, 55). At the initial times of immersion, corrosive ions do not have enough times to pass through the coating. By passing the time, phase angle regarding SHP Mg alloy decreased due to the penetration of aggressive species in the protective NiO layer. However, at each time of immersion, $θ_{10\ kHz}$ and $|Z|_{100\ mHz}$ corresponding to SHP Mg alloy showed the higher magnitude than that of bare Mg alloy due to its better corrosion resistance. As observed $|Z|_{100\ mHz}$ reduced from 2.5 to 1.1 MΩ cm² and 290 to 65 Ω cm² for SHP Mg and Mg alloy, respectively. Besides, $θ_{10\ kHz}$ related SHP Mg decreased from 81 to 70°, while the values of this parameter corresponding to Mg alloy changed from 7 to 2°, which could be due to the effect of superhydrophobic layer on the surface of Mg alloy.
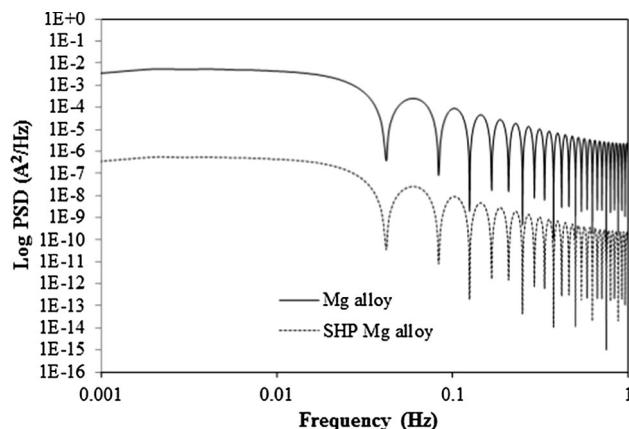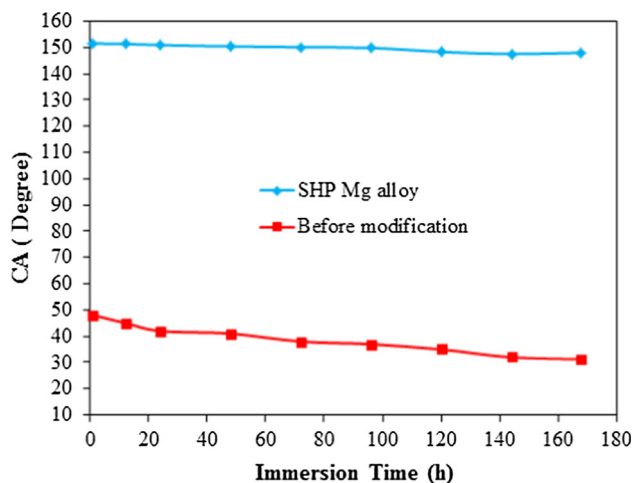

Fig. 9 Water contact angle regarding the surface of Mg alloy before and after modification by stearic acid
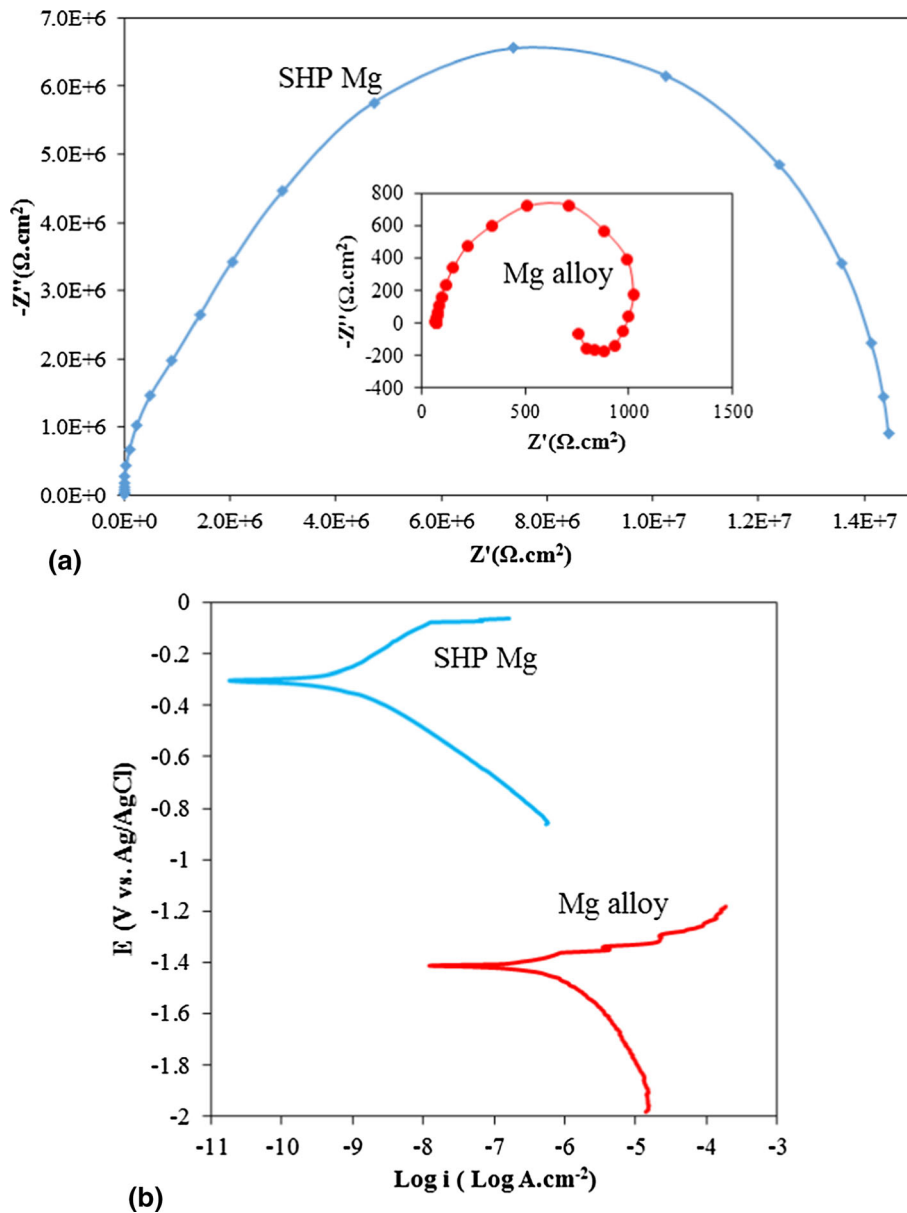
Fig. 10 (a) Nyquist and (b) potentiodynamic polarization plots regarding SHP Mg alloy and Mg alloy after immersion of 1 h in the deionized water

Figure 7 demonstrates potentiodynamic polarization plots corresponding to Mg alloy and SHP Mg in the 3.5 wt.% NaCl solution. Corrosion current density (I_{corr}) regarding SHP Mg alloy and Mg alloy was estimated about 1.47 nA cm^{-2} and 82.7 µA cm^{-2}, respectively. As it can be seen, corrosion current density of SHP Mg was lower of about three orders of magnitude than that of Mg sample. The lower corrosion current density of SHP Mg shows the higher corrosion density of this sample in the chloride media. Besides, corrosion potential of SHP Mg was recorded much more positive than Mg sample. It could be attributed to the higher mobility of surface regarding SHP Mg. As stated earlier, NiO phase formed on the surface of Mg by chemical treatment. It could act as a barrier against corrosive species and water molecules and, therefore, the corrosion resistance of SHP Mg shows the higher value in comparison with Mg.

Figure 8 shows power spectral density (PSD) of current related to SHP Mg alloy and Mg alloy after 1 h of immersion in 3.5 wt.% NaCl solutions. In the case of Mg alloy, more severe corrosion can result from the higher PSD (I) values. Therefore, a drop in the noise level could represent a lower electrochemical activity (Ref 56, 57). The better behavior of SHP Mg alloy could be evidenced by using a quantity denoted as noise resistance (R_n). This parameter was calculated from the ratio of the standard deviations of voltage fluctuations divided by the identical amount of current variations. The higher R_n value shows the higher corrosion resistance of mentioned surface (Ref 56, 57). The calculated R_n for SHP Mg alloy and Mg alloy after 1 h of immersion in the NaCl solution obtained 709 and 0.501 kΩ cm^2, respectively. Therefore, it could be shown that the corrosion resistance of SHP Mg alloy was greater than Mg alloy as the EIS and polarization tests emphasized this behavior.
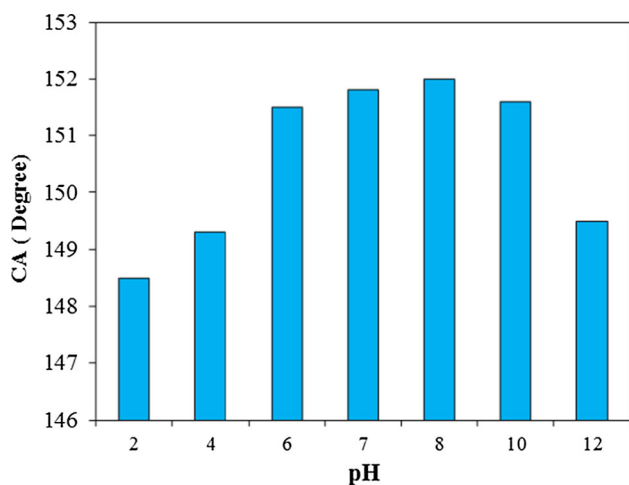
Fig. 11 Contact angle of SHP Mg at different pHs

Figure 9 shows the relationship between the water contact angle of SHP Mg alloy and the surface before modification by stearic acid with the exposure time. The CA on the surface only slightly decreased to 149.5° from 151.5° after the exposure time of 168 h, while for the untreated sample with stearic acid this value decreased from 49 to 33°. This phenomenon demonstrates that superhydrophobic surfaces have long-term stability, and this will improve the corrosion resistance of magnesium alloy as mentioned before. However, the density of the hydrophobic functional groups on the surface could be decreased by immersing the samples in the NaCl solution, which led to the reduction in contact angle by passing the time. This can indicate that on most parts of the sample surface desorption of the SA molecules or degradation of the flake-like morphology occurred (Ref 33, 58).

Figure 10(a) and (b) illustrates Nyquist spectra and potentiodynamic polarization plots corresponding to Mg alloy and SHP Mg alloy after immersion 1 h in the deionized water. According to Fig. 10(a), Mg alloy showed a semicircle plot which was related to the charge transfer response followed by the induction loop in the low-frequency region. In the case of SHP Mg, the inductive loop was disappeared which indicated the significant reduction in electrolyte penetration to the interface. R_{ct} for Mg alloy after immersion 1 h in the water was obtained as 830 Ω cm^2. This parameter for SHP Mg alloy reported as 12 MΩ cm^2, which could be explained by the effect of superhydrophobicity behavior on the surface of Mg alloy. The higher reported R_{ct} in the water solution compared 3.5 wt.% NaCl solution could be due to the aggressive behavior of chloride ion exposing the surface. Figure 10(b) shows potentiodynamic polarization plots corresponding to Mg alloy and SHP Mg in the water solution. Corrosion current density (I_{corr}) regarding SHP Mg alloy and Mg alloy was estimated about 0.27 nA cm^{-2} and 27 μA cm^{-2}, respectively. As it can be observed, corrosion current density of SHP Mg was much lower than that of Mg alloy, which stated earlier.

Figure 11 illustrates the relationship between the contact angle and the pH value regarding SHP Mg. Contact angles (CA) varied from 148.5° to 152° in the pH range of 2-12, which emphasizes the relative chemical stability of superhydrophobic film under the strong acidic or basic environment. The CA declination from 150° in strong acidic (pH 2) and basic (pH 12) environment could be associated with the loss of air pockets

(Ref 59). The lower CA at aggressive media (pH 2 or 12) could be due to the non-homogeneous formation of superhydrophobic film due to the presence of two α phase (Mg) and β phase (Mg$_{17}$Al$_{12}$) (Ref 7). These distinct phases could result in the formation of uneven thickness layer on the surface and, therefore, provide the relative susceptibility of the surface toward the penetration of massive aggressive ions.

4. Conclusion

In this work, superhydrophobic Mg alloy was synthesized by the immersion of Mg plates in the CuCl$_2$/NiSO$_4$ solution following by SA modifier. Modified Mg alloy showed a contact angle of 151.5°, which attributed to the flake-like morphology with nano-sized thickness. This parameter reduced to 149.5° after 168 h of immersion in the NaCl solution. Besides, due to the prevention of water droplet diffusion to the coating, SHP Mg showed a significant corrosion resistance in the chloride media. I_{corr} regarding SHP Mg recorded more than four orders of magnitude lower than AZ31 Mg alloy. In addition, noise resistance and R_{ct} regarding the SHP Mg alloy possessed the greater values compared to Mg alloys, which was due to the presence of resistant phase of NiO and superhydrophobic tail of stearic species on the surface. Although, SHP Mg showed a contact angle ranged from 148°-152° at the different pHs.

References

1. A. Atrens, G.L. Song, M. Liu, Z.M. Shi, F.Y. Cao, and M.S. Dargusch, Review of Recent Developments in the Field of Magnesium Corrosion, *Adv. Eng. Mater.*, 2015, **17**, p 400–453

2. Z. Kang and W. Li, Facile and Fast Fabrication of Superhydrophobic Surface on Magnesium Alloy by One-Step Electrodeposition Method, *J. Ind. Eng. Chem.*, 2017, **50**, p 50–56

3. M. La, H. Zhou, N. Li, Y. Xin, R. Sha, S. Bao, and P. Jin, Improved Performance of Mg-Y Alloy Thin Film Switchable Mirrors After Coating with a Superhydrophobic Surface, *Appl. Surf. Sci.*, 2017, **403**, p 23–28

4. G. Song, A. Atrens, G. Song, and A. Atrens, Recent Insights into the Mechanism of Magnesium Corrosion and Research Suggestions, *Adv. Eng. Mater.*, 2007, **9**, p 177–183

5. X.B. Chen, N. Birbilis, and T.B. Abbott, Effect of [Ca^{2+}] and [PO$_4$$^{3-}$] Levels on the Formation of Calcium Phosphate Conversion Coatings on Die-Cast Magnesium Alloy AZ91D, *Corros. Sci.*, 2012, **55**, p 226–232

6. R. Udhayan and D.P. Bhatt, On the Corrosion Behavior of Magnesium and Its Alloys Using Electrochemical Techniques, *J. Power Sources*, 1996, **53**, p 103–107

7. Z. Wang, Q. Li, Z. She, F. Chen, L. Li, X. Zhang, and P. Zhang, Facile and Fast Fabrication of Superhydrophobic Surface on Magnesium Alloy, *Appl. Surf. Sci.*, 2013, **271**, p 182–192

8. J. Senf and E. Broszeit, Wear and Corrosion Protection of Aluminum and Magnesium Alloys Using Chromium and Chromium Nitride PVD Coatings, *Adv. Eng. Mater.*, 1999, **1**, p 133–137

9. G. Wu, X. Zeng, and G. Yuan, Growth and Corrosion of Aluminum PVD-Coating on AZ31 Magnesium Alloy, *Mater. Lett.*, 2008, **62**, p 4325–4327

10. Z.C. Wang, F. Jia, L. Yu, Z.B. Qi, Y. Tang, and G.-L. Song, Direct Electroless Nickel–Boron Plating on AZ91D Magnesium Alloy, *Surf. Coat. Technol.*, 2012, **206**, p 3676–3685

11. D. Seifzadeh and Z. Rajabalizadeh, Environmentally-Friendly Method for Electroless Ni-P Plating on Magnesium Alloy, *Surf. Coat. Technol.*, 2013, **218**, p 119–126

12. E. Georgiza, J. Novakovic, and P. Vassiliou, Characterization and Corrosion Resistance of Duplex Electroless Ni-P Composite Coatings on Magnesium Alloy, *Surf. Coat. Technol.*, 2013, **232**, p 432–439

13. J. Liang, P.B. Srinivasan, C. Blawert, M. Störmer, and W. Dietzel, Comparison of Electrochemical Corrosion Behaviour of MgO and ZrO$_2$ Coatings on AM50 Magnesium Alloy Formed by Plasma Electrolytic Oxidation, *Corros. Sci.*, 2009, **51**, p 2483–2492

14. P.B. Srinivasan, J. Liang, C. Blawert, M. Störmer, and W. Dietzel, Effect of Current Density on the Microstructure And Corrosion Behaviour of Plasma Electrolytic Oxidation Treated AM50 Magnesium Alloy, *Appl. Surf. Sci.*, 2009, **225**, p 4212–4218

15. Z. Yao, Y. Xu, Y. Liu, D. Wang, Z. Jiang, and F. Wang, Structure and Corrosion Resistance of ZrO$_2$ Ceramic Coatings on AZ91D Mg Alloys by Plasma Electrolytic Oxidation, *J. Alloys Compd.*, 2011, **509**, p 8469–8474

16. Y. Chen, B.L. Luan, G.-L. Song, Q. Yang, D.M. Kingston, and F. Benseba, An Investigation of New Barium Phosphate Chemical Conversion Coating on AZ31 Magnesium Alloy, *Surf. Coat. Technol.*, 2012, **210**, p 156–165

17. G. Wang, M. Zhang, and R. Wu, Molybdate and Molybdate/Permanganate Conversion Coatings on Mg-8.5 Li Alloy, *Appl. Surf. Sci.*, 2012, **258**, p 2648–2654

18. X. Wang, L. Zhu, X. He, and F. Sun, Effect of Cerium Additive on Aluminum-Based Chemical Conversion Coating on AZ91D Magnesium Alloy, *Appl. Surf. Sci.*, 2013, **280**, p 467–473

19. T. Masanari and S. Hiromoto, Growth Mechanism of Hydroxyapatite-Coatings Formed on Pure Magnesium and Corrosion Behavior of the Coated Magnesium, *Appl. Surf. Sci.*, 2011, **257**, p 8253–8257

20. R. Rojaee, M. Fathi, and K. Raeissi, Electrophoretic Deposition of Nanostructured Hydroxyapatite Coating on AZ91 Magnesium Alloy Implants with Different Surface Treatments, *Appl. Surf. Sci.*, 2013, **258**, p 664–673

21. S. Sonmez, B. Aksakal, and B. Dikici, Influence of Hydroxyapatite Coating Thickness and Powder Particle Size on Corrosion Performance of MA8M Magnesium Alloy, *J. Alloys Compd.*, 2014, **456**, p 125–131

22. R.-G. Hu, S. Zhang, J.-F. Bu, C.-J. Lin, and G.-L. Song, Recent Progress in Corrosion Protection of Magnesium Alloys by Organic Coatings, *Prog. Org. Coat.*, 2012, **73**, p 129–141

23. L. Xu and A. Yamamoto, In vitro Degradation of Biodegradable Polymer-Coated Magnesium Under Cell Culture Condition, *Appl. Surf. Sci.*, 2012, **258**, p 6353–6358

24. M. Yeganeh and M. Saremi, Corrosion Inhibition of Magnesium Using Biocompatible Alkyd Coatings Incorporated by Mesoporous Silica Nanocontainers, *Prog. Org. Coat.*, 2015, **79**, p 25–30

25. X. Zhang, G. Wu, X. Peng, L. Li, H. Feng, B. Gao, K. Huo, and P.K. Chu, Mitigation of Corrosion on Magnesium Alloy by Predesigned Surface Corrosion, *Sci. Rep.*, 2015, **5**, p 1–11

26. P.R. Cha, H.S. Han, G.F. Yang, Y.C. Kim, K.H. Hong, S.C. Lee, J.Y. Jung, J.P. Ahn, Y.Y. Kim, S.Y. Cho, J.Y. Byun, K.S. Lee, S.J. Yang, and H.K. Seok, Biodegradability Engineering of Biodegradable Mg Alloys: Tailoring the Electrochemical Properties and Microstructure Of Constituent Phases, *Sci. Rep.*, 2013, **3**, p 2367–2372

27. M. Nosonovsky and B. Bhushan, *Multiscale Dissipative Mechanisms and Hierarchical Surfaces*, Springer, Berlin, 2008

28. Z. Guo, W. Liu, and B.-L. Su, Superhydrophobic Surfaces: From Natural to Biomimetic to Functional, *J. Colloid Interface Sci.*, 2011, **353**, p 335–355

29. M. Yeganeh and N. Mohammadi, Superhydrophobic Surface of Mg Alloys: A Review, *J. Magn. Alloys*, 2018, **6**(1), p 59–70

30. Y. Liu, J.D. Liu, S.Y. Li, J.A. Liu, Z.W. Han, and L.Q. Ren, Biomimetic Superhydrophobic Surface of High Adhesion Fabricated with Micronano Binary Structure on Aluminum Alloy, *ACS Appl. Mater. Interface*, 2013, **5**, p 8907–8914

31. F. Zhang, C. Zhang, L. Song, R. Zeng, S. Li, and H. Cui, Fabrication of the Superhydrophobic Surface on Magnesium Alloy and Its Corrosion Resistance, *J. Mater. Sci. Technol.*, 2015, **31**, p 1139–1143

32. L. Feng, Y. Zhu, W. Fan, Y. Wang, X. Qiang, and Y. Liu, Fabrication and Corrosion Resistance of Superhydrophobic Magnesium Alloy, *Appl. Phys. A*, 2015, **120**, p 561–570

33. T. Ishizaki and N. Saito, Rapid Formation of a Superhydrophobic Surface on a Magnesium Alloy Coated with a Cerium Oxide Film by a Simple Immersion Process at Room Temperature and Its Chemical Stability, *Langmuir*, 2010, **26**, p 9749–9755

34. Y. Liu, X. Yin, J. Zhang, S. Yu, Z. Hana, and L. Ren, A Electro-Deposition Process for Fabrication of Biomimetic Super-Hydrophobic Surface and Its Corrosion Resistance on Magnesium Alloy, *Electrochim. Acta*, 2014, **125**, p 395–403

35. Y. Liu, J.Z. Xue, D. Luo, H.Y. Wang, X. Gong, Z.W. Han, and L.Q. Ren, One-Step Fabrication of Biomimetic Superhydrophobic Surface by Electrodeposition on Magnesium Alloy and Its Corrosion Inhibition, *J. Colloid Interface Sci.*, 2017, **491**, p 313–320

36. Y. Liu, G. Lu, J. Liu, Z. Han, and Z. Liu, Fabrication of Biomimetic Hydrophobic Films with Corrosion Resistance on Magnesium Alloy by Immersion Process, *Appl. Surf. Sci.*, 2013, **264**, p 527–532

37. Z. Qiu, J. Sun, R. Wang, Y. Zhang, and X. Wu, Magnet-Induced Fabrication of a Superhydrophobic Surface on ZK60 Magnesium Alloy, *Surf. Coat. Technol.*, 2016, **286**, p 246–250

38. S.V. Gnedenkov, V.S. Egorkin, S.L. Sinebryukhov, I.E. Vyaliy, A.S. Pashinin, A.M. Emelyanenko, and L.B. Boinovich, Formation and Electrochemical Properties of the Superhydrophobic Nanocomposite Coating on PEO Pretreated Mg-Mn-Ce Magnesium Alloy, *Surf. Coat. Technol.*, 2013, **232**, p 240–246

39. Z. Kang, X. Lai, J. Sang, and Y. Li, Fabrication of Hydrophobic/Super-Hydrophobic Nanofilms on Magnesium Alloys by Polymer Plating, *Thin Solid Film*, 2011, **520**, p 800–806

40. H. Wang, Y. Weia, M. Liang, L. Hou, Y. Li, and C. Guo, Fabrication of Stable and Corrosion-Resisted Super-Hydrophobic Film on Mg Alloy, *Colloid Surf. A Physicochem. Eng. Asp.*, 2016, **509**, p 351–358

41. W. Xu, J. Song, J. Sun, Y. Lu, and Z. Yu, Rapid Fabrication of Large-Area, Corrosion-Resistant Superhydrophobic Mg Alloy Surfaces, *ACS Appl. Mater. Interfaces*, 2011, **3**, p 4404–4414

42. M. Liang, Y. Wei, L. Hou, H. Wang, and C. Guo, Fabrication of a Super-Hydrophobic Surface on a Magnesium Alloy by a Simple Method, *J. Alloys Compd.*, 2016, **656**, p 311–317

43. A.B.D. Cassie and S. Baxter, Surface Roughness and Contact Angle, *Trans. Faraday Soc.*, 1944, **40**, p 546–551

44. F. Song, C. Wu, H. Chen, Q. Liu, J. Liu, R. Chen, R. Li, and J. Wang, Water-Repellent and Corrosion-Resistance Properties of Superhydrophobic and Lubricant-Infused Super Slippery Surfaces, *RSC Adv.*, 2017, **7**, p 44239–44246

45. H. Feng, S. Liu, Y. Du, T. Lei, and T. Yuan, Effect of the Second Phases on Corrosion Behavior of the Mg-Al-Zn Alloys, *J. Alloys Compd.*, 2017, **695**, p 2330–2338

46. S.-Y. Han, D.-H. Lee, Y.-J. Chang, S.-O. Ryu, T.-J. Lee, and C.-H. Chang, The Growth Mechanism of Nickel Oxide Thin Films by Room-Temperature Chemical Bath Deposition, *J. Electrochem. Soc.*, 2006, **153**, p 382–386

47. H. Wan and X. Hu, One-Step Solve-Thermal Process for the Construction of Anticorrosion Bionic Superhydrophobic Surfaces on Magnesium Alloy, *Mater. Lett.*, 2016, **174**, p 209–212

48. W.F. Ng, M.H. Wong, and F.T. Cheng, Stearic Acid Coating on Magnesium for Enhancing Corrosion Resistance in Hanks' Solution, *Surf. Coat. Technol.*, 2010, **204**, p 1823–1830

49. C. Wu, Q. Liu, R. Chen, J. Liu, H. Zhang, R. Li, K. Takahashi, P. Liu, and J. Wang, Fabrication of ZIF-8@SiO$_2$ Micro/Nano Hierarchical Superhydrophobic Surface on AZ31 Magnesium Alloy with Impressive Corrosion Resistance and Abrasion Resistance, *ACS Appl. Mater. Interface*, 2017, **9**, p 11106–11115

50. M. Saremi and M. Yeganeh, Application of Mesoporous Silica Nanocontainers as Smart Host of Corrosion Inhibitor in Polypyrrole Coatings, *Corros. Sci.*, 2014, **86**, p 159–170

51. A.D. King, N. Birbilis, and J.R. Scully, Accurate Electrochemical Measurement of Magnesium Corrosion Rates; A Combined Impedance, Mass-Loss and Hydrogen Collection Study, *Electrochim. Acta.*, 2014, **121**, p 394–406

52. M. Yeganeh, M. Eskandari, and S.R. Alavi-Zaree, A Comparison Between Corrosion Behaviors of Fine-Grained and Coarse-Grained Structures of High-Mn Steel in NaCl Solution, *J. Mater. Eng. Perform.*, 2017, **26**, p 2484–2490

53. J. Jayaraj, S.A. Raj, A. Srinivasan, S. Ananthakumar, U.T.S. Pillai, N.G.K. Dhaipule, and U.K. Mudali, Composite Magnesium Phosphate Coatings for Improved Corrosion Resistance of Magnesium AZ31 Alloy, *Corros. Sci.*, 2016, **113**, p 104–115

54. A. Keyvani, M. Yeganeh, and H. Rezaeyan, Electrodeposition of Zn-Co-Mo Alloy on the Steel Substrate from Citrate Bath and Its Corrosion Behavior in the Chloride Media, *J. Mater. Eng. Perform.*, 2017, **26**, p 1958–1966

55. A. Keyvani, M. Yeganeh, and H. Rezaeyan, Application of Mesoporous Silica Nanocontainers as an Intelligent Host of Molybdate Corrosion Inhibitor Embedded in the Epoxy Coated Steel, *Prog. Nat. Sci. Mater. Int.*, 2017, **27**, p 261–267

56. R. Naderi and M.M. Attar, Effect of Zinc-Free Phosphate-Based Anticorrosion Pigment on the Cathodic Disbondment of Epoxy-Polyamide Coating, *Prog. Org. Coat.*, 2014, **77**, p 830–835

57. B.P. Markhali, R. Naderi, M. Mahdavian, M. Sayebani, and S.Y. Arman, Electrochemical Impedance Spectroscopy and Electrochemical Noise Measurements as Tools to Evaluate Corrosion Inhibition of Azole Compounds on Stainless Steel in Acidic Media, *Corros. Sci.*, 2013, **75**, p 269–279

58. T. Ishizaki, Y. Masuda, and M. Sakamoto, Corrosion Resistance and Durability of Superhydrophobic Surface Formed on Magnesium Alloy Coated with Nanostructured Cerium Oxide Film and Fluoroalkylsilane Molecules in Corrosive NaCl Aqueous Solution, *Langmuir*, 2011, **27**, p 4780–4788

59. J. Yuan, J. Wang, K. Zhang, and W. Hu, Fabrication and Properties of a Superhydrophobic Film on an Electroless Plated Magnesium Alloy, *RSC Adv.*, 2017, **7**, p 28909–28917